Lamellar Diblock Copolymer Grain Boundary Morphology. 3. Helicoid Section Twist Boundary Energy

Samuel P. Gido*

Polymer Science and Engineering Department, University of Massachusetts, Amherst, Massachusetts 01003

Edwin L. Thomas*

Program in Polymer Science and Technology, Department of Material Science and Engineering, Massachusetts Institute of Technology, Cambridge, Massachusetts 02139

Received February 22, 1996; Revised Manuscript Received April 1, 1997[⊗]

ABSTRACT: The helicoid section morphology allows a diblock copolymer lamellar phase to maintain microphase separation across a twist grain boundary. The interface between the two microphases in the grain boundary region approximates a stack of sections of the helicoid minimal surface. Grain boundary energies were calculated for the helicoid section morphology both as a function of diblock chain characteristics and as a function of grain boundary twist angle. The basic approach to grain boundary energy calculation is to formulate a general expression for local free energy density as a function both of chain characteristics and of the local curvature of the interface. The local energy density is then integrated over the mathematical model for the Scherk grain boundary. Two general methods of calculation were used, and the results where then compared. First, a self-consistent field model was formulated in which average energies per chain were calculated for all the possible interfacial curvature environments encountered by diblocks in the helicoid section morphology. A second general approach utilized a continuum (Helfrich) model for interfacial deformation in which moduli are used to impose energetic penalties for curvature of the interface in the grain boundary region. The helicoid section grain boundary energies were compared to energies of a competing twist boundary morphology, the Scherk surface, which was analyzed in the preceding paper of this series. It was found that the energies of both the Scherk morphology and the helicoid section increase with increasing twist. The Scherk and helicoid section energies are comparable at low twist angles, less than about 15°. Both morphologies are observed in this twist range. For higher twist angles, where only the Scherk morphology is observed, the helicoid section boundary energy becomes prohibitively high due to a compression of the lamellar layers.

I. Introduction

Diblock copolymer materials which form microphase-separated morphologies such as spheres, cylinders, tricontinuous cubics, and lamellas also form larger scale grain structures. The specific structure of the boundary regions between grain has a great impact on material properties, such as elastic modulus and gas permeability, that depend on the continuity of the individual phases across the grain boundaries. This paper is the third in a series of four papers on the grain boundary morphology of lamellar diblock copolymers.[1−3] In the first paper of the series,[1] which we denote GB-I, twist grain boundary morphologies in lamellar diblock copolymers were characterized using transmission electron microscopy (TEM). Two specific twist grain boundary morphologies were observed: the helicoid section, observed at low twist angles, and Scherk's first surface, observed over the entire twist angle range from 0 to 90°. Figure 1 reviews the basic geometry of a twist grain boundary and shows the definition of the twist angle α. Figure 4 of GB-I shows the continuous twist deformation of a lamellar material that constitutes the helicoid section boundary and also shows how a section of the helicoid minimal surface is used to model the interface between the two diblock microphases in the grain boundary region. Grain boundary energy calculations were performed for the Scherk surface morphology in the second paper, GB-II.[2] In the present paper, grain boundary energy calculations are performed for the helicoid section morphology and compared with previous results for the Scherk morphology.

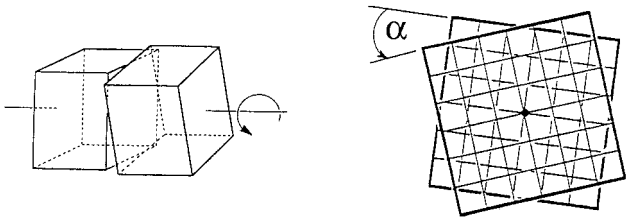

Figure 1. A twist grain boundary is produced by twisting adjacent grains of material by an angle α about a common axis.

The helicoid grain boundary energy calculations are carried out for three different SB diblocks: molecular weights 20 500/20 500, 42 300/45 400, and 81 000/74 400 (designated SB 20/20, 40/40, and 80/80). These are the same symmetric, lamella-forming diblocks that were used in the TEM grain boundary characterization work presented in GB-I. The χN values for these three samples at the annealing temperature of 110−120 °C are about 50, 100, and 200. Thus, our use of strongly segregated models for calculation of grain boundary energy is clearly justified for SB 40/40 and 80/80. SB 20/20 is only in intermediate segregation, so the use of strong segregation models represents an approximation in this case.

The global equilibrium structure of a sample of lamellar diblock copolymer would be a single, macroscopic, lamellar pseudocrystal. However, multigrained structures are commonly observed in TEM micrographs, such as GB-I Figure 1 and GB-II Figure 2. Section II of GB-II gives a discussion of possible physical processes leading to grain structure formation. Given that grains exist, it seems reasonable to assume that the material in the narrow grain boundary regions assumes a local

[⊗] Abstract published in *Advance ACS Abstracts,* June 1, 1997.

S0024-9297(96)00303-8 CCC: $14.00

equilibrium structure within the constraints imposed by the orientations of the adjoining bulk lamellar grains. The assumption of local equilibrium in the grain boundary region is supported by the consistent observation of the same two twist boundary morphologies, Scherk and helicoid section.

Energies are calculated as a function of the response of the diblock chains to their geometrical environment in the grain boundary morphology. One aspect of the grain boundary geometry is the curvature of the intermaterial dividing surface (IMDS). (As in GB-I and GB-II, the intermaterial dividing surfaces in the grain boundary regions, and in other defect structures, have been designated IMDS† to distinguish them from the interfacial surfaces in equilibrium microdomain morphologies, which are designated simply IMDS.) The local geometry of the IMDS† at a point on the surface is fully specified by the two principal curvatures, c_1 and c_2, which are the reciprocals of the two principal radii of curvature at that point. The average of the two principal curvatures is called the mean curvature, $H = (c_1 + c_1)/2$, while their product is called the Gaussian curvature, $K = c_1c_2$. In the case of grain boundary structures, there are additional geometric constraints, besides IMDS† curvature, that are required by the twist reorientation of the grain boundary.

H and K are the working representations of IMDS† geometry used to model the effect of IMDS† curvature on diblock chain energy. For the Scherk morphology energy calculations in GB-II, two approaches to the calculation of the effect of this IMDS† geometry on local diblock energy were considered: The most general method is to explicitly calculate the equilibrium diblock layer characteristics and free energy at every point (actually a finite element mesh of points) on the intermaterial dividing surface using a self-consistent field (SCF) theory. The second approach is to work by analogy to the classical theory of elasticity of membranes and express the free energy of the diblock interface at each point in terms of energy penalties (expressed as moduli) for deviations from the preferred or natural interfacial curvature. Flat planes are the preferred interfacial shape for lamella-forming, symmetric diblock copolymers.

The most general grain boundary energy calculations are carried out by solving the SCF model[4−6] for the chain conformation distribution and local energy density at a point on the IMDS† as a function of the local values of H and K. This local energy density must then be integrated over the IMDS†. Using a piecewise linear approximation for the chain end distribution function, we are able to get numerical solutions to the SCF model for diblock melts as a function of arbitrary local curvature.[7] Since the helicoid section surface is a minimal surface the only geometrical parameter that changes from point to point on the surface, is K. We were able to calculate the total energy per chain vs K with the SCF model. Chain energy vs K was then fit by a relatively simple analytical function that we proceeded to integrate over the helicoid IMDS† to give grain boundary energies.

If the deviations of a diblock layer from its preferred curvature can be modeled with a continuum elasticity theory, then a considerably simplified working expression for the curvature-induced free energy density increase can be obtained. When applied to lamellar diblocks,[8−13] this general approach leads to the following form of the free energy, f, in a deformed lamella:

$$f = f_o + kH^2 + \bar{k}K \tag{1}$$

Equation 1 may be formulated to give energy per unit interfacial area, as is common in its application to microemulsions. However, due to the variability in the area per diblock chain on the IMDS with curvature, Wang and Safran have formulated a model using an expression of the same form to give an energy per chain. The form of eq 1 shown here is for the particular case, relevant to our diblock copolymer lamellar systems, in which the natural or preferred curvature of the layers is zero (flat planes). In eq 1, f_o is the free energy per unit area or per chain of the minimum energy flat diblock interface, while H and K characterize the deviations from the flat interface up to a second-order dependence on curvature. k is the splay modulus, and $\bar{k}$ is the saddle-splay modulus. The helicoid section IMDS† is a minimal surface. Thus, $H = 0$, so that the second term on the right-hand side of eq 1 drops out. Wang and Safran[10−12] present an approach for the calculation of the curvature moduli, k and $\bar{k}$, for diblock copolymers which is discussed in GB-II. In all our calculations, K is made dimensionless by multiplying by $(h^*)^2$, where h^* is the equilibrium thickness of a flat grafted brush. The flat brush thickness is equal to one-quarter of the lamellar long period, L.

Before proceeding, however, it is necessary to more closely examine the applicability of the Wang and Safran work to our grain boundary morphologies. The Wang and Safran theory is strictly applicable only for an isolated diblock layer. It assumes that the only important energy contributions are interfacial and chain-stretching energies from that single layer. There are no external constraints other than the curvature that the layer is assumed to possess. However, our grain boundary morphologies impose additional geometric constraints that are not accounted for in the Wang and Safran model. In GB-II, it was found that additional geometric constraints in the Scherk surface twist boundary morphology lead to different results from those predicted by Wang and Safran. In the Scherk surface energy calculations, the interfacial curvature effects and the additional grain boundary geometry requirements were closely coupled to one another, and thus both effects were taken into account in the Scherk specific SCF grain boundary energy calculations. In the helicoid section morphology, however, the curvature energy and the effects of the other grain boundary geometric requirements are essentially uncoupled from one another, because they act on spatially separated regions of the IMDS†.

II. Helicoid Section Grain Boundary Geometry

The following is an analytical formula for the helicoid IMDS†:

$$(x, y, z) = (r\cos\phi, r\sin\phi, s\phi) \tag{2}$$

$$0 \le \phi \le \alpha, \quad 0 \le r \le D/2$$

$$s = 2\pi/\text{pitch} = \text{function}(D, \text{molecular parameters})$$

Here, α is the twist angle of the boundary. The parameter, r, is the radius of the helicoid, i.e., the distance from the helicoid axis (z-axis) to any point on the surface. The maximum value of r is limited to the half-width of the grain, $D/2$, where D is the grain size.

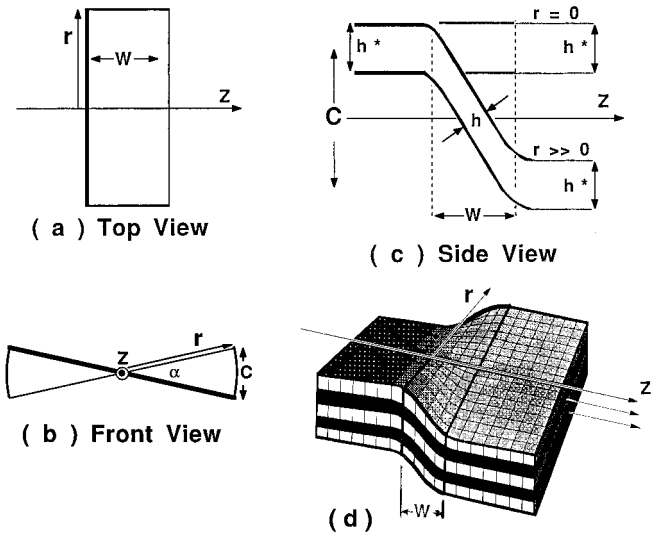

Figure 2. Geometry of the helicoid section grain boundary as seen from three different directions: (a) top, (b) front, and (c) side. The perspective view (d) links the three directional views. The *z*-axis of the helicoid is shown in each view. The boundary width, *W*, the twist angle, α, the displacement, *C*, of the lamellar layers across the boundary, and the radial coordinate, *r*, are shown. *C* depends on the radial distance from the *z*-axis: $C = 2r \sin(\alpha/2)$. In the side view (c), it is apparent that, as *C* increases, the height, *h*, of the polymer brush grafted to the IMDS† in the grain boundary region decreases from the flat lamellar equilibrium value $h^* = L/4$. The side view shows that, at $r = 0$, there is no compression of the lamellar layers in the boundary region, but for $r \gg 0$, there is significant compression.

The parameter *s* determines the relationship between the rate of rotation of the generating line (line A in GB-I Figure 3b) and the rate of its translation along the *z*-axis: pitch $= 2\pi/s$. The value of the parameter *s* has been experimentally determined from TEM micrographs in GB-I. Using elementary differential geometry,[14] *H* and *K* can then be calculated at any point on these surfaces.[7] *K* on the helicoid interface is a function of radius, *r*, and the scale factor, *s*:

$$K = -s^2/(s^2 + r^2)^2 \qquad (3)$$

Since the helicoid is a minimal surface, these calculations yield $H = 0$ and $K \leq 0$ for all points on the IMDS†.

Helicoid section geometrical calculations are done with energy normalized by kT and length measured in dimensionless "mathematical units". Mathematical units, abbreviated mu, are defined such that one long period of the lamellar structure is equal to 2π mu. The dimensionless mu length unit is necessary when using eqs 2 and 3 to describe the helicoid section grain boundary model. Lamellar long periods, *L*, for the three diblocks used in this study were determined by small-angle X-ray scattering (SAXS) in order to obtain the following relationships between physical and mathematical length units for each polymer: $L(20/20) = 387$ Å $= 2\pi\ \mathrm{mu}_{20/20}$, $L(40/40) = 625$ Å $= 2\pi\ \mathrm{mu}_{40/40}$, and $L(80/80) = 1060$ Å $= 2\pi\ \mathrm{mu}_{80/80}$.

Figure 2 shows the geometry of the helicoid section boundary viewed from three different directions: top (Figure 2a), front (Figure 2b), and side (Figure 2c). Figure 2d is a perspective view of the helicoid section boundary that links these three directional views. The width of the boundary region, *W*, is equal to *s*α. The *z*-axis and radial direction, *r*, are indicated in the top and front views. The side view illustrates an important geometrical consequence of the twist boundary geometry. The lamellas in the helicoid section twist boundary are sheared in such a way that their thickness, *h*, is reduced from the equilibrium layer thickness, *h**, observed in the flat lamella. As illustrated in the figure, this reduction in thickness occurs due to the geometry of connecting lamellar layers that have been sheared past one another by the twist of the boundary. The amount of this shear displacement is shown as *C* in Figure 2c. *C* increases with increasing radial position and with increasing twist angle: $C = 2r \sin(\alpha/2)$. The width *W* over which this displacement occurs also affects the compression of the lamellar layers. Thus, the reduction in lamellar thickness at a given point in the boundary depends on *W*, α, and r, according to the following geometrical relationship:

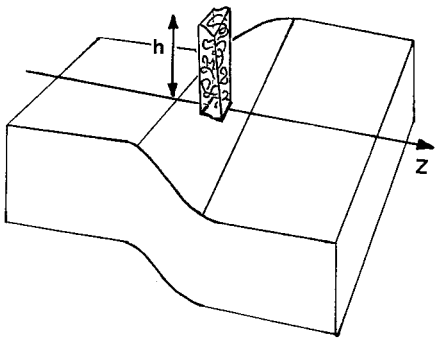

Figure 3. Volume element occupied by one diblock copolymer chain tethered to a helicoid section-shaped IMDS†.

$$h/h^* = \sin\left[\tan^{-1}\left(\frac{W}{2r \sin(\alpha/2)}\right)\right] \qquad (4)$$

The compression of the lamellar layers from their equilibrium thickness gets increasingly more severe as the radial distance from the *z*-axis increases, as the twist angle increases, and as the boundary width decreases. The *r* dependence will be shown to limit the radial extent, *D*/2, of these boundaries. The compression of the lamellar layers with increasing twist is responsible for the experimental fact that these boundaries are observed only at low twist angles, up to about 15°. Finally, the *W* dependence of layer compression prohibits very narrow helicoid section boundaries. Experimentally, these boundaries are quite wide: *W*/*L* is about 3−4.

The energy due to the curvature of the helicoid section IMDS† is concentrated in a relatively small "core" region at small *r* values, near the *z*-axis of the helicoid. The energy due to the compression of the lamellar layers is negligible in this small *r* core region. The compression energy becomes large for larger *r* values, remote from the *z*-axis. In this region, the curvature energy is negligible. Thus, we can calculate grain boundary energies by combining a core energy due to interfacial curvature, at approximately constant lamellar thickness, with an energy due to compression of essentially flat lamellar layers at larger *r* values.

III. Core Region Curvature Energy Calculations

The effects of IMDS† curvature on chain conformation and interfacial area per chain, Σ, are now considered for the core region. Through conservation of volume, Σ is directly linked to the height, *h*, of the grafted layer of diblock chains. Figure 3 shows a portion of diblock interface with the helicoid section geometry and a

polymer chain confined to an imaginary volume element. This element has area Σ at the interface. The area of a two-dimensional slice through this volume element, parallel to the surface, at a height h above the surface, is $\Sigma(h) = (1 + hc_1)(1 + hc_2)\Sigma = (1 + 2Hh + Kh^2)\Sigma$. The conservation of volume constraint for a single chain is[5]

$$\int_0^h \Sigma(h)\, dh = N_A v \tag{5}$$

where N_A is the degree of polymerization of the block on the side of the interface under consideration, and v is the volume per monomer. Thus, the product $N_A v$ is the volume of the A block, V_A. Evaluation of this simple integral gives a cubic equation relating h and Σ:

$$\frac{1}{3}Kh^3 + Hh^2 + h - \frac{N_A v}{\Sigma} = 0 \tag{6}$$

Equations 5 and 6 are general conservation of volume results that must always relate Σ and h.

In the helicoid section, the geometrical constraints of the grain boundary fix the values of h and thus Σ at values somewhat different than those obtained from the Wang and Safran theory (GB-II eq 2). Thus, we will use a helicoid-specific, ground state-dominant SCF (HsSCF) model to calculate energies per chain in the core region. From eq 4, it is found that the layer thickness remains at essentially h^* throughout the core region. For instance, at $r/L = 1$, which will be shown to be a very conservative estimate for the radial extent of the core region, $h/h^* = 0.998$. Solution of eq 6 with $h = h^*$, $H = 0$, and $K \neq 0$ yields a relationship for Σ on a helicoid section interface in the core region:

$$\Sigma = N_A v\left[\frac{1}{3}K\left(\frac{N_A v}{\Sigma^*}\right)^3 + \frac{N_A v}{\Sigma^*}\right]^{-1} = V_A\left[\frac{1}{3}K(h^*)^3 + h^*\right]^{-1} \tag{7}$$

Equation 7 indicates a larger increase in Σ/Σ^* with increasing $|K|$ than in the Wang and Safran case. In GB-II section IV, it was found that, for $K > 0.506$, the Wang and Safran relationship for Σ as a function of K, eq 2, becomes unphysical due to the inability accommodate the diblock chains in the space available near the curved IMDS†. This problem persists when the Wang and Safran model is applied to the helicoid section geometry. Additionally, this difficulty occurs for the HsSCF solution employing eq 7 when $|K| > 1.0$. However, Gaussian curvatures high enough for the geometric model to become unphysical were not encountered in the helicoid section grain boundaries that were actually observed in the TEM.

The details of the application of the SCF model to arbitrarily curved interfaces in diblock melts are provided elsewhere.[7] The key to the solution of this problem is to determine a chain end distribution function $g(x')$ such that the conformational energy per chain,

$$\Delta F_{el} = \frac{3}{2}\int_0^h g(x')\left(\int_0^{x'} E(x,x')\, dx\right) dx' \tag{8}$$

is minimized with respect to constraints such as conservation of volume and constant segmental density. Here, x' denotes the position of the free end of a grafted chain. $E(x,x')$ is the local chain-stretching energy at point x of a grafted chain. Thus, the inner integral represents the total chain-stretching energy for a grafted chain with its end at x'. The outer integral then computes an average conformational energy per chain by summing over the brush height and weighting each energy by $g(x')$.

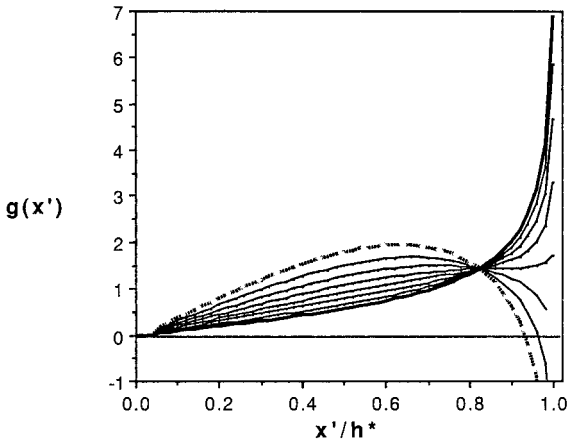

Figure 4. Chain end distribution functions $g(x')$ for various K values in the helicoid section grain boundary geometry. The family of curves progresses from the bold curve ($K = 0.0$) to the dotted curve ($K = -1.0$) in increments of -0.2. These plots are independent of molecular weight when distance from the interface is measured in dimensionless units, x'/h^*. At $K = 0$, the greatest concentration of chain ends is at or near the full brush height. With increasing $|K|$, although the brush height remains constant, more chain ends become distributed throughout the brush. For $|K| > 1$, a dead zone indicated by negative $g(x')$ values develops at the top of the brush, indicating a breakdown in the model at these higher interfacial curvatures.

Figure 4 shows the chain end distribution functions, $g(x')$, calculated with our numerical solution technique for various K values. These profiles, plotted vs the dimensionless length x'/h^*, are independent of molecular weight. Although the brush height does not change with increasing $|K|$, due to the constraints of the helicoid boundary geometry, the shape of the $g(x')$ curves, as $|K|$ increases, follows a pattern of evolution similar to that found for brushes on the concave side of a cylinder.[6] The pattern displayed by both the cylindrically grafted chains and the chains on the helicoid section IMDS† involves a transition from a distribution where the chain ends are concentrated near the edge of the brush, for the flat case, to a situation where the more of the chain ends are distributed throughout the brush as $|K|$ increases. On the concave side of a cylinder, as well as in the helicoid section case, this change in chain end distribution with increasing curvature (H for the cylinder and K for the helicoid) is a response to the decrease in available space to locate chain ends near the full brush height. This is evident, for instance, in GB-II Figure 4.

Chain end distributions determined by the HsSCF analysis were then used in eq 8 to determine the total elastic energy per chain. The total energy per chain, F_{tot}, is equal to the sum of the elastic energy plus an interfacial energy term equal to $\gamma\Sigma$. In our HsSCF calculations, we employ an average Kuhn length a of 6 Å, approximately applicable to both the PS and PB blocks. We take $v = 140$ Å^3, which is the average of the PS and PB volumes per monomer, 100 and 180 Å^3, respectively. The interfacial energy, γ, was calculated from χ using the following relationship:[10,16] $\gamma = a\chi^{1/2}/v$. χ is a function of T and was calculated using the relationship[17] $\chi = -0.0937 + 66/T$, which gives a value of 0.074 at the annealing temperature of 120 °C. This gives a γ value at this temperature of 0.012 kT/Å^2.

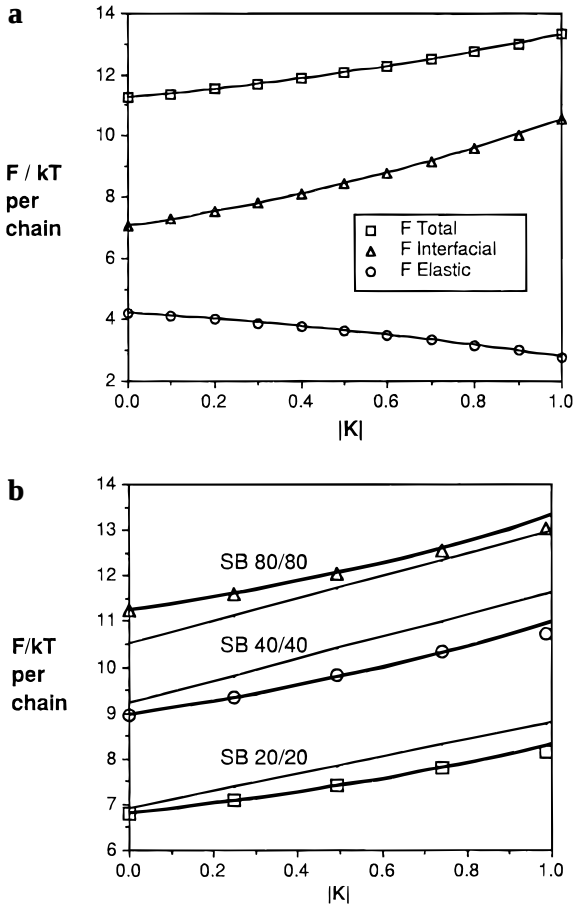

Figure 5. Plots of energy per chain as a function of $|K|$. (a) Plots of chain-stretching and interfacial component energies as well as total energy per chain for SB 80/80 as a function of $|K|$. The chain-stretching energy decreases from 4.2 to 2.8 kT/chain as $|K|$ increases from 0 to 1. Over the same curvature range, the interfacial energy per chain increases from 7.0 to 10.5 kT. This leads to an overall increase in total energy per chain from 11.2 to 13.3 kT. The general trends displayed in this plot for SB 80/80 are also found in similar graphs (not shown) for SB 20/20 and 40/40. (b) Average total energy per chain vs $|K|$ for SB 20/20, 40/40, and 80/80. HsSCF average total energy per chain, F_{tot}, is plotted as the bold curves. The symbols are Scherk twist boundary total energies per chain, shown for comparison, calculated with a Scherk-specific SCF model (SB 80/80, △; SB 40/40, ○; SB 20/20, □). The light lines are Wang and Safran energies per chain.

Figure 5a shows the elastic energy, interfacial energy, and total energy per chain on the helicoid section interface in the core region ($r/L \leq 1$) for SB 80/80 as a function of $|K|$. Although the brush height is held constant at h^*, the average stretching energy per chain decreases from 4.2 to 2.8 kT as $|K|$ increases from 0 to 1. The decrease in stretching energy with increasing $|K|$ occurs due to the change in the shape of the chain end distribution evident in Figure 4. Over the same $|K|$ range, the interfacial energy per chain for SB 80/80 increases from 7.0 to 10.5 kT due to the increase in Σ. This leads to an increase in total energy per chain with increasing $|K|$.

We can now compare energies per chain, as a function of K, calculated with the HsSCF model and the Wang and Safran model. The application of the Wang and Safran model to grain boundary morphologies is discussed in greater detail in GB-II. Figure 5b shows a comparison of the HsSCF and Wang and Safran dependence for energy per chain on K for the helicoid section morphology. Over the range of $|K|$ from 0 to 1, the dependence is remarkably similar for all three molecular weight diblocks.

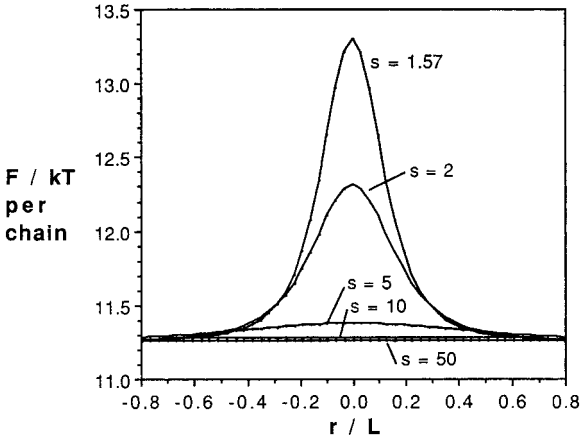

Figure 6. Free energy density maps of the helicoid section IMDS† for SB 80/80. The energy on the helicoid surface depends only on the radial distance, r, from the z-axis. The local energy per chain in kT units is plotted vs r/L for values of s ranging from 1.57 to 50 mu/rad.

Figure 6 shows plots of free energy density vs r/L for helicoid section boundaries in SB 80/80. The maximum energy per chain occurs on the z-axis of the helicoid, where $r = 0$, and the energy falls off quite rapidly with increasing r/L. Most of the excess energy, over the flat interface energy per chain of 11.2 kT, is concentrated into a region of about 1 L in width, centered on the z-axis. The height of this energy maximum increases with decreasing s. A smaller s value indicates a faster turning helicoid, which involves higher interfacial curvature and thus higher energy. The height of the free energy density peak around $r = 0$ falls very rapidly as s increases. Experimentally, s is actually quite large, on the order of 100 (GB-I). For such large s values, the increase in energy due to IMDS† curvature is very small, essentially negligible. For this reason, we can neglect the curvature energy in the helicoid section core region. Essentially all the energy associated with this type of boundary comes from the compression of the lamellar layers at larger r values.

IV. Lamellar Layer Compression Energy Calculations

The compression of the lamellar layers from their equilibrium thickness, h^*, as a function of W, α, and r, is given by eq 4. Experimentally, it is known from GB-I that helicoid section boundaries are observed at low twist angles, up to about 15°; 10° twist boundaries, which are commonly observed, have boundary widths of about $W/L = 3$. The grain size observed in these samples was about 2−5 μm for all three molecular weights. Thus, the maximum radial extent of helicoid section grain boundaries must be on the order of 1−3 μm. The independent effects of the variables W, α, and r on h/h^* are investigated in the plots shown in Figure 7, where two of the variables are held constant at typically observed experimental values and the third is varied over a wide range. In Figure 7a, the boundary width is fixed at $W/L = 3$, and the radial position is fixed at $r/L = 16$. In absolute units, this radial position is 0.6 μm in SB 20/20, 1 μm in SB 40/40, and 1.7 μm in SB 80/80. The layer thickness, h/h^*, at this radial distance from the z-axis is shown in this plot to decrease rapidly with increasing twist angle. At a twist of about 20°, for instance, the layer is compressed to about half its equilibrium thickness.

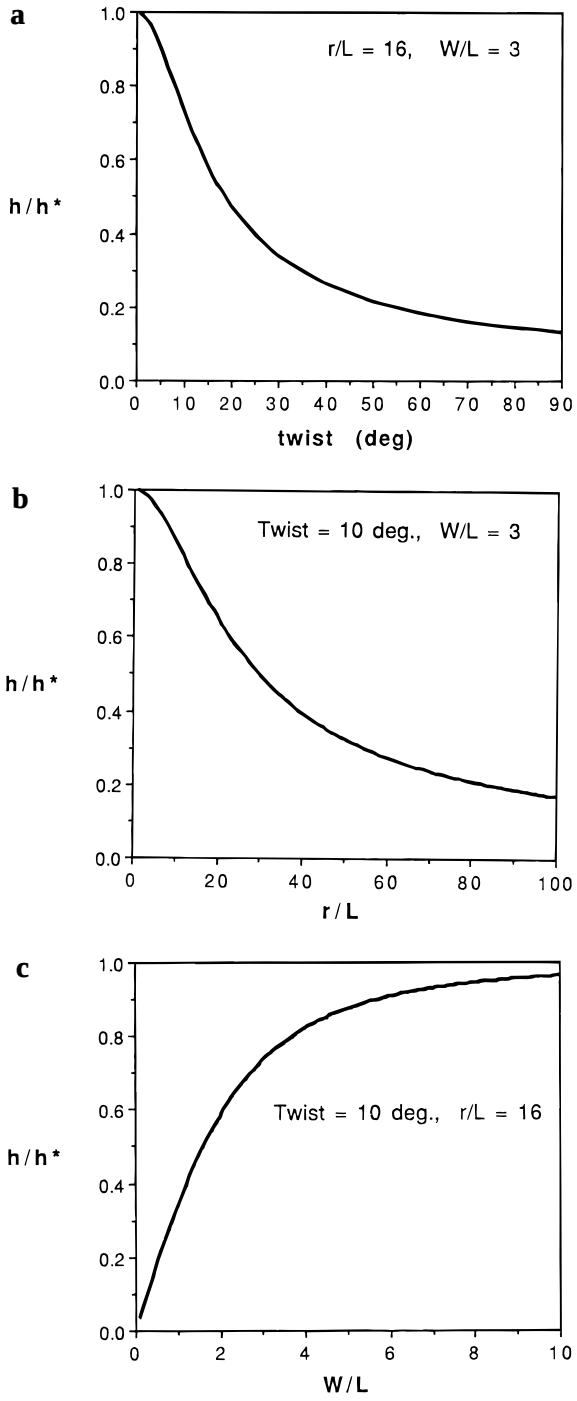

Figure 7. Plots of h/h^* as a function of twist angle, radial position, and grain boundary width. (a) h/h^* vs twist angle at radial position $r/L = 16$ and for fixed boundary width $W/L = 3$. (b) h/h^* vs radial position r/L for a twist angle of 10° and for fixed boundary width $W/L = 3$. (c) h/h^* vs boundary width W/L at radial position $r/L = 16$ and for a twist angle of 10°.

Figure 7b shows a plot of h/h^* vs r/L for a fixed twist of 10° and a fixed boundary width of $W/L = 3$. The layer thickness decreases rapidly with increasing radial distance from the helicoid core. For instance, at a distance of $r/L = 30$, the layer thickness is reduced to half of its equilibrium value. Finally, Figure 7c shows a plot of h/h^* vs W/L for a fixed twist of 10° and a fixed radial position of $r/L = 16$. Layer thickness approaches 1 as W/L becomes large. As the boundary width gets smaller, layers become increasingly compressed. The compression is relatively weak down to widths of about $W/L = 3$, where the layers still maintain about 75% of their equilibrium thickness. However, decreasing the width below this leads to a sharp decrease in lamellar thickness.

In the large r region, where the lamellar compression is significant, the helicoid section IMDS† is essentially flat. As h/h^* decreases from 1, the chain conformational energy first falls to zero as chain stretching is relaxed and then increases as the chains become compressed. As the lamellas are compressed and the chain dimension normal to the interface is reduced, the area per chain on the IMDS†, and thus the interfacial energy, are correspondingly increased. The ground state dominant SCF model that was used in the core region and for the Scherk surface morphology cannot be used to calculate the energy per chain associated with lamellar compression because the assumption of ground state dominance requires the chains to be strongly stretched normal to the IMDS†. To get a qualitative feel for the compression energy in the helicoid section boundary, we will use an Alexander−de Gennes type scaling relationship for the chain conformational energy:

$$F = F_{\mathrm{i}} + F_{\mathrm{cS}} + F_{\mathrm{cB}} \tag{9}$$

F_{i} is the interfacial energy per chain at the PS−PB interface, given by $F_{\mathrm{i}} = \gamma\Sigma$. F_{cS} and F_{cB} are conformational energies per chain for the PS and PB blocks, respectively. They are approximated by the following expression:[18−20,22]

$$F_{cj} = \frac{3}{2}\,kT\left[\left(\frac{R_j}{\mathrm{R}_{j\mathrm{o}}}\right)^2 + \left(\frac{R_{j\mathrm{o}}}{R_j}\right)^2 - 2\right] \tag{10}$$

where j is either S or B for the PS and PB blocks. R_j is the end-to-end distance of block j in the microphase-separated morphology. In the Alexander−de Gennes formalism, this end-to-end distance is taken as the thickness of the layer in the structure corresponding to block j. For our lamellar systems, this corresponds to the brush height, $h = L/4$, which is the approximately the same for both the PS and PB blocks. $R_{j\mathrm{o}}$ is the ideal Gaussian chain end-to-end distance of the j block, which is the reference state for chain conformational energy, and which is given by $a_j N_j^{1/2}$, where N_j is the degree of polymerization of block j and a_j is the statistical segment length of the polymer in block j. The simple scaling relationship for the free energy per chain, given by eqs 9 and 10, is accurate to within a constant factor of order unity.[21]

Figure 8 shows conformational, interfacial, and total energy per chain as a function of h/h^* in SB 80/80. The total energy per chain for the flat interface in this plot is somewhat lower than the value given by the SCF model, 8.5 kT as opposed to 11.2 kT. This difference is due to the qualitative nature of the Alexander−de Gennes scaling approach. Nevertheless, this approach will allow us to ascertain the important effects of grain boundary geometry on energy. As expected, the conformational energy falls to zero as the initial chain stretching is relieved and then increases dramatically as the layer becomes compressed. The interfacial energy increases monotonically with decreasing h/h^*. The total energy increases very slowly as h/h^* is decreased slightly, since in this region of the plot the decreasing conformational energy partially compensates for the increasing interfacial energy. Once the conformational energy starts to rise again for stronger layer compression, it adds to the increasing interfacial energy

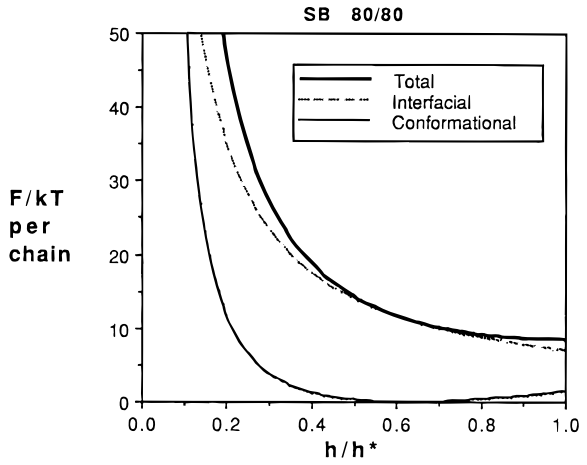

Figure 8. Conformational, interfacial, and total energy per chain as a function of h/h^*, calculated using the Alexander–de Gennes scaling form of the free energy.

and results in a rapid increase in total energy per chain for further decreasing h/h^*.

Combining our knowledge of the dependence of h/h^* on helicoid section boundary geometry, as illustrated in Figure 7, with the dependence of energy per chain on h/h^*, shown in Figure 8, the energy per chain is obtained as a function of W, r, and α. Figure 9a shows the total energy per chain at a radial distance from the z-axis $r/L = 16$, for a boundary width $W/L = 3$, as a function of twist. The energy increases slightly as twist increases from 0° to about 10 or 15°. For higher twists, the energy rises more rapidly with increasing twist. The three curves in the figure are for SB 20/20, 40/40, and 80/80 in order of increasing energy. Since grains routinely reach sizes that require helicoid section radial extents of $r/L = 16$ or greater, it is clear that this increase in energy with increasing twist places an upper limit on the twist angles for which the helicoid section morphology can occur. The transition from a slowly increasing to a more rapidly increasing energy with increasing twist which occurs around 15° is approximately coincident with the upper limit of the range in which helicoid section boundaries are experimentally observed.

Figure 9b shows the total energy per chain in a 10° helicoid section boundary of width $W/L = 3$, as a function of r/L. The three curves in the figure are for SB 20/20, 40/40, and 80/80 in order of increasing energy. Clearly, the increasing energy with increasing radial distance from the z-axis limits the size of helicoid section boundaries. The energy starts to increase sharply for r/L larger than about 20. Of course, boundaries of larger radial extent may be able to lower their energy somewhat by widening a little more. Due to the projection angles required to see a helicoid section boundary in TEM, we have no way of actually measuring the radial extent of a helicoid section boundary. However, we know from the average grain size of the materials examined that radial extents of 20–30 must occur in the materials, but that very large radial extents above about 50, which produce prohibitively high energies, do not occur.

Figure 9c shows the total energy per chain in a 10° helicoid section boundary at a radial distance from the z-axis of $r/L = 16$ vs W/L. The three curves in the figure are for SB 20/20, 40/40, and 80/80 in order of increasing energy. The energy is very high for boundary widths less than about $W/L = 2$. Just above $W/L = 3$, the

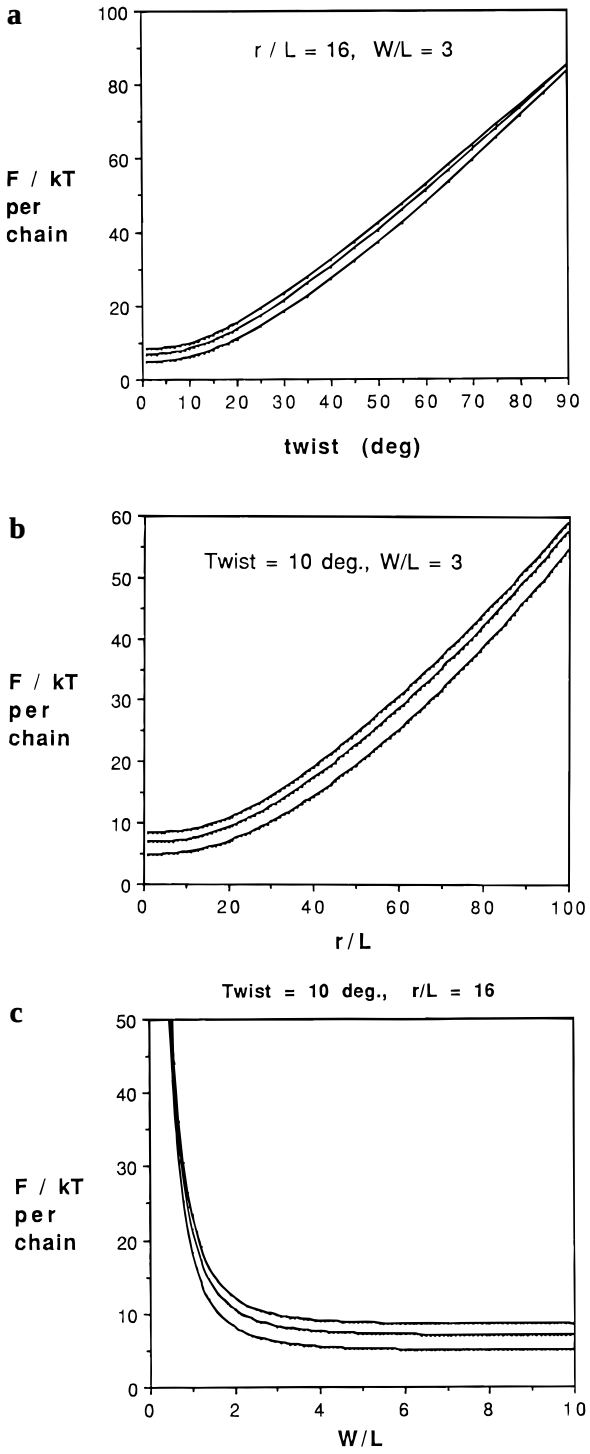

Figure 9. Plots of total energy per chain as a function of twist angle, radial position, and grain boundary width. (a) Total energy per chain vs twist at a radial position of $r/L = 16$ and for a fixed boundary width of $W/L = 3$. The three curves are for SB 20/20, 40/40, and 80/80 in order of increasing energy. (b) Total energy per chain vs r/L for a 10° helicoid and for a fixed boundary width of $W/L = 3$. The three curves are for SB 20/20, 40/40, and 80/80 in order of increasing energy. (c) Total energy per chain vs boundary width, W/L, for a 10° helicoid section at a radial position of $r/L = 16$. The three curves are for SB 20/20, 40/40, and 80/80 in order of increasing energy.

energy essentially reaches a constant low value. From this figure, it is clear that 10° helicoid sections of radial extent $r/L = 16$ or greater should, at least, be wider than $W/L = 2$. This is consistent with the experimentally observed width of $W/L \approx 3$. Helicoid section boundaries that are formed with initial widths smaller than $W/L \approx$

2 are expected to widen in order to lower their lamellar compression energy.

V. Conclusions

This paper concludes our investigation of twist grain boundaries in lamellar diblock copolymers that began with the TEM characterization work in GB-I. Two twist boundary morphologies were experimental discovered and theoretically investigated: the Scherk saddle surface morphology and the helicoid section morphology. GB-II was concerned with energy calculations for the Scherk surface morphology. In the present paper, the grain boundary energy calculation techniques that were introduced in GB-II are applied to the helicoid section twist boundary morphology. The increase in energy per chain in the grain boundary morphologies results from changes in the area per chain on the IMDS[†] and in the chain conformations induced by the curvature of the interface. In the helicoid section case, we also needed to consider changes in chain conformation and interfacial energies resulting from compression of the lamellar layers. Both the helicoid sections and Scherk IMDS[†]'s are minimal surfaces, so that mean curvature, H, is equal to zero everywhere on the interface. Thus, for both the Scherk morphology and the core region of the helicoid section, energies are calculated as a function of the Gaussian curvature, K. The Helfrich form of the free energy gives the energy of a curved ampiphilic layer in terms of penalties, quantified by moduli, for mean and Gaussian curvature. Since diblock copolymers are macromolecular amphiphile analogs, Wang and Safran have applied this type of expression to curvature of diblock copolymer layers with the moduli calculated using a SCF model. In the present study, we have found that the Wang and Safran approach is not rigorously applicable to curved interfaces in the twist grain boundary morphologies because the interfaces involved must interact with one another as they pack together to fulfill the geometric requirements of the grain boundary. Thus, for both the Scherk morphology and the core region of the helicoid section, we have specified these additional geometric constraints and solved Scherk-specific and helicoid-specific SCF models that have taken them into account.

It was found that the helicoid section core energy due to interfacial curvature is negligible with respect to the lamellar compression energy that occurs at larger radial distances from the z-axis of the helicoid. This lamellar compression results in very high energies for boundaries with widths, W/L, less than about 2 or 3, thus explaining the $W/L = 3$ boundary width observed experimentally. The energies of helicoid section grain boundaries are relatively low for low twist angles, but lamellar compression results in a dramatic increase in energy as twist becomes larger. This dramatic increase in energy roughly corresponds to the 15° cutoff angle, above which helicoid section boundaries were not experimentally observed. At higher twist angles, only the Scherk surface morphology is observed.

Acknowledgment. We thank Dr. L. J. Fetters of Exxon for synthesizing the diblock copolymers. Discussions with the following individuals are acknowledged: Profs. H. Karcher, D. Hoffman, R. Kusner, P. Smith, and A. S. Argon. Funding was provided by NSF-DMR 92-14853 and AFOSR F49620-94-1-0224.

References and Notes

(1) Gido, S. P.; Gunther, J.; Thomas, E. L.; Hoffman, D. *Macromolecules* **1993**, *26*, 4506 (referred to herein as GB-I).
(2) Gido, S. P.; Thomas, E. L. *Macromolecules* **1994**, *27*, 849 (referred to herein as GB-II).
(3) Gido, S. P.; Thomas, E. L. *Macromolecules* **1994**, *27*, 6137 (referred to herein as GB-IV).
(4) Milner, S. T.; Witten, T. A.; Cates, M. E. *Macromolecules* **1988**, *21*, 2610.
(5) Semenov, A. N. *Sov. Phys. JETP* **1985**, *61*, 733.
(6) Zhulina, E. B.; Liatskaya, Y. V.; Birshtein, T. M. *Polymer* **1992**, *33*, 332.
(7) Gido, S. P. Chemical Engineering Ph.D Thesis, Massachusetts Institute of Technology, 1993.
(8) Frank, F. C. *Discuss. Faraday Soc.* **1958**, *25*, 19.
(9) Helfrich, W. *Z. Naturforsch.* **1973**, *28*, 693.
(10) Wang, Z.-G.; Safran, S. A. *J. Phys.* **1990**, *51*, 185.
(11) Wang, Z.-G.; Safran, S. A. *Europhys. Lett.* **1990**, *11*, 425.
(12) Wang, Z.-G.; Safran, S. A. *J. Chem. Phys.* **1991**, *94*, 679.
(13) Kléman, M. *Proc. R. Soc. London* **1976**, *347*, 387.
(14) Struik, D. J. *Lectures on Classical Differential Geometry*, 2 ed.; Dover: New York, 1961; pp 61, 62.
(15) Milner, S. T.; Witten, T. A. *J. Phys.* **1988**, *49*, 1951.
(16) Helfand, E.; Tagami, Y. *J. Chem. Phys.* **1972**, *56*, 3592.
(17) Mori, K.; Hasegawa, H.; Hashimoto, T. *Polym. J.* **1985**, *17*, 799.
(18) Alexander, S. *J. Phys.* **1977**, *38*, 977.
(19) de Gennes, P. G. *J. Phys.* **1976**, *37*, 1443.
(20) de Gennes, P. G. *Macromolecules* **1980**, *13*, 1069.
(21) Milner, S. T. *Science* **1991**, *251*, 905.
(22) Leibler, L.; Orland, H.; Wheeler, J. C. *J. Chem. Phys.* **1983**, *79*, 3550.

MA9603037